A novel fuel cell design for operando energy-dispersive X-ray absorption measurements

IOP Publishing Journal Title
Journal **XX** (XXXX) XXXXXX https://doi.org/XXXX/XXXX

A novel fuel cell design for *operando* energy-dispersive X-ray absorption measurements

A.S. Leach[1], J. Hack[1], M. Amboage[2], S. Diaz-Moreno[2], H. Huang[3], P.L. Cullen[1,4], M. Wilding[5], E. Magliocca[1], T. S. Miller[1], C. A. Howard[6], D.J.L. Brett[1], P.R. Shearing[1], P.F. McMillan[7], A.E. Russell[3] and R. Jervis[1]*

[1] Electrochemical Innovation Lab, Department of Chemical Engineering, UCL, London WC1E 7JE, United Kingdom
[2] Diamond Light Source, Didcot, Oxon, OX11 0DE, United Kingdom
[3] School of Chemistry, University of Southampton, University Road, Southampton SO17 1BJ, United Kingdom
[4] School of Engineering and Materials Science (SEMS) and Material Research Institute, Queen Mary University of London, London, E1 4NS, United Kingdom
[5] UK Catalysis Hub, Research Complex at Harwell, Harwell Campus, OX11 0FA.
[6] Department of Physics & Astronomy, University College London, London WC1E 6BT, United Kingdom
[7] Department of Chemistry, Christopher Ingold Laboratory, University College London, 20 Gordon St., London WC1H 0AJ, United Kingdom

E-mail: rhodri.jervis@ucl.ac.uk

Received xxxxxx
Accepted for publication xxxxxx
Published xxxxxx

Abstract

A polymer electrolyte fuel cell (PEFC) has been designed to allow *operando* X-ray absorption spectroscopy (XAS) measurements of catalysts. The cell has been developed to operate under standard fuel cell conditions, with elevated temperatures and humidification of the gas-phase reactants, both of which greatly impact the catalyst utilisation. X-ray windows in the endplates of the cell facilitate collection of XAS spectra during fuel cell operation while maintaining good compression in the area of measurement. Results of polarisation curves and cyclic voltammograms (CVs) showed that the *operando* cell performs well as a fuel cell, while also providing XAS data of suitable quality for robust XANES analysis. The cell has produced comparable XAS results when performing a cyclic voltammogram to an established *in situ* cell when measuring the Pt LIII edge. Similar trends of Pt oxidation, and reduction of the formed Pt oxide, have been presented with a time resolution of 5 seconds for each spectrum, paving the way for time-resolved spectral measurements of fuel cell catalysts in a fully-operating fuel cell.

Keywords: Polymer electrolyte fuel cell (PEFC); Platinum; *Operando*; XAS; XANES

1. Introduction

Polymer electrolyte fuel cells (PEFCs) have the potential to transform global transport networks, contribute to a zero carbon emissions future and move fast refuelling electric vehicles to widespread adoption. There are, however, challenges to overcome including improvement of the efficiency of the oxygen reduction reaction (ORR) as well as the durability of the catalysts while continuing to reduce the

amount of Pt required in a fuel cell stack, and therefore the overall cost.[1] Major funding organisations, such as the U.S. Department of Energy (DoE), are targeting a system cost of $30/kW by 2025, which is less than 25% of that of current commercially deployed technology.[2]

The catalysts used in fuel cells have a key influence on their overall performance and combined studies of the catalyst redox processes under realistic electrochemical cycling conditions are necessary to realise the improvements in electrocatalyst formulation and behaviour. X-ray absorption spectroscopy (XAS) with high energy X-rays is a versatile technique for studying the properties of fuel cell catalysts that provides information about the electronic structure and redox state of transition metals through changes in the near-edge region of the spectra (X-ray absorption near-edge structure, XANES). It can also provide structural information about the local ordering of atoms via analysis of the extended X-ray absorption fine structure (EXAFS) region of the spectrum, while these atoms are undergoing redox changes during the electrocatalytic process.[3] The XAS technique is element-specific, with each electron transition being responsible for a well-defined, abrupt increase in absorption at or around the 'edge' energy. By carefully tuning the incident beam energy it is possible to study several different elements contained within the same sample of alloy catalysts.[4–6] When XAS experiments are combined with an *in situ* cell that allows for electrochemical control, the change in the spectra of fuel cell catalysts with varying potential provides vital information about their electronic and local structural properties during redox reactions of interest such as the ORR.[7,8] Fast time-resolved XAS is a powerful technique for understanding the transient processes occurring at the catalysts. Whereas time resolution of several minutes is needed to measure XAS with conventional step-scanning XAS, sub-second time scales are achieved with energy-dispersive or quick-scanning XAS, allowing observation and interpretation of faster processes.[9–12]

The I20-EDE beamline at Diamond Light Source, UK, is dedicated to energy-dispersive XAS, with the capability of collecting a complete absorption spectrum with a time resolution down to microseconds in transmission detection mode. [13–15] The beamline uses an energy-dispersed beam, with a broad range of energies simultaneously irradiating the sample, and together with a position sensitive detector to allow the whole energy spectrum to be collected in a single shot, in contrast with scanning beamlines where the energy scan is performed in a sequential mode by adjusting the monochromator angle. The beamline can also be operated in 'turbo-XAS' mode, whereby a narrow horizontal slit is scanned through the energy-dispersed fan of radiation, selecting a monochromatic beam.[16] During the turbo-XAS measurements, the slit is scanned in a continuous manner at fast speed, while the detectors are triggered at selected slit position/energy intervals. When using this arrangement, spectra can also be collected in fluorescence detection mode, enabling experiments in dilute samples with second time resolution.

When benchmarking the characteristics of fuel cell catalysts using a classical three-electrode approach, it is not clear how the aqueous environment compares to a realistic triple-phase boundary involving the gas-phase reactants in contact with a solid membrane electrolyte and catalyst surface in a fuel cell set-up.[17] For example, in some aqueous-phase three-electrode based measurements under load cycle conditions, degradation mechanisms associated with particle migration and coalescence have been observed.[18] This contrasts with membrane electrode assembly (MEA) tests that have only reported Pt dissolution, but not migration or coalescence.[19] This highlights the fact that it is of the utmost importance to perform characterisation of the electrocatalyst behaviour under realistic *operando* conditions, as the electrode layer in an aqueous rotating disc electrode, or even a model MEA environment, differs substantially from that experienced by a real working fuel cell electrode. Factors such as the binder chosen for the thin-film layer can have a substantial impact on the measured performance in an aqueous test environment.[20] It is therefore important to move towards the evaluation of catalysts in real working fuel cells (or as close as possible), by employing gas diffusion electrodes and truly *operando* environments.[21]

Among the few examples of *operando* studies using X-ray spectroscopy of fuel cell catalysts there are several reports from the Tada group[22–24] using a bespoke cell with Kapton windows at SPring-8 synchrotron facility (Japan), and a cell that was developed by the Russell group for use at Daresbury Laboratory (UK) and the ESRF (France).[25,26] The cell used by the Tada group was optimised for computed tomography (CT) and incorporates a long thin slit across the whole width of the cell, allowing measurements that are taken at 10 degrees incidence to the plane of the electrode, across a channel in the flow field.

In this paper, preliminary results using a novel *operando* fuel cell geometry specifically designed for XAS to provide a realistic fuel cell performance are reported. The results are compared to XAS data obtained using a more established aqueous cell design employed in previous studies.[7,8,27] This cell design implemented at the I20 EDE beamline is shown here to be effective for assessing the catalytic response during cyclic voltammetry experiments, and could pave the way for future studies of time-dependent processes occurring in real operating fuel cells.

2. Methods: Design of Cell and Experimental Conditions

A cell was designed for carrying out the *operando* measurements, as shown in an exploded view in Figure 1(a), and manufactured by GGM Engineering (Sussex, UK). The MEA, of area 5 cm^2, sits at the centre of the cell, surrounded by gaskets for gas sealing, flow field plates (machined from a graphite composite bipolar plate material), gold-coated copper current collectors and insulated aluminium end-plates. The cathode (left) and anode (right) contain X-ray windows at the centre, for *operando* imaging in either transmission or fluorescence detection mode, the former shown by the position of the source and detector in Figure 1(b). This cell will be designated as the "*operando"* cell in this work. These X-ray transparent windows are created by the removal of the current collector and end-plate material in this area, and a thin layer of bipolar plate material maintains good compression with reduced X-ray attenuation in the measurement region. Overall compression of the cell is provided via tie-rods in the endplates than in turn compress the bipolar plate material, which is rigid and therefore translates this compression of the MEA over the measurement window, ensuring good electrical contact in the area of spectroscopic measurement. This differentiates the cell presented in this work from those previously published, as previously published cells use Kapton windows [22-24] where the area of MEA measured will have reduced compression and therefore will not be in a representative environment of the whole cell. Additionally, the window position allows spatially resolved measurements to be conducted perpendicular to the MEA, at different points along the flow field or in channels or land area. Compression in the area of spectroscopic measurement is vital as this can have a drastic effect on local fuel cell performance.[26,28] Local areas of poor electrochemical performance might not impact on the overall performance of the MEA (and thus go unnoticed in the averaged electrochemical behaviour of the fuel cell),[29] but could cause the area of XAS measurement to be less electrochemically active and thus give an inaccurate picture of the true changes in the catalyst from the spectra collected. The large bevel on the cathode X-ray window facilitates data acquisition in fluorescence mode by enabling collection of a greater solid angle of the emitted X-rays, without interference from the end-plate. The graphite plates are interchangeable, so a variety of flow field designs can be manufactured and employed and easily incorporated into the design. For the experiments discussed here, the graphite composite bipolar plates had an interdigitated design on both anode and cathode with a channel depth of 0.5 mm. In the X-ray window region discussed above, the bipolar plate thickness was 0.5 mm in the channel region and 1 mm in the land region. For spectra collection in transmission mode, the beam was positioned in a channel region to minimise the amount of material that the beam travelled through.

Contained within the insulated end-plates are holes for cartridge heaters and a thermocouple, allowing the cell to be heated to a desired temperature using PID control. Gas inlet and outlets are affixed to the end-plates, with gas lines connected via 1/4 in Swagelok fittings. Both air and nitrogen are available to flow over the cathode, which allows cyclic voltammetry (CV) measurements to be carried out on the cell. Gases on the anode and cathode were supplied at a fixed flow rate of 100 mL min^{-1} and were bubbled through de-ionised water heated to 50 °C before entering the cell, acting as humidifiers. The de-ionised water was contained within Duran flasks held within a water bath, with a set-point of 50 °C, which was monitored using a thermometer. Gas lines were insulated to maintain the temperature and minimise condensation on the walls of the tubing. The cell temperature was set at 50 °C using a PID temperature controller (Omega, US) and the cell was heated using cartridge heaters inserted into the end plates of the cell, meaning the device was operated at 100% relative humidity. Current collection is carried out by attaching potentiostat cables to the tabs on either the current collector plates or directly onto the graphite plates themselves. A 3D -printed cell holder was used to mount the cell onto the beamline (Figure 1(b)), with the cathode positioned to the front (i.e., facing the X-ray source) and the anode positioned to the rear. Three alignment screws on the front and back of the holder screwed directly into the sample stage, such that the cell sat in an identical position during each scan.

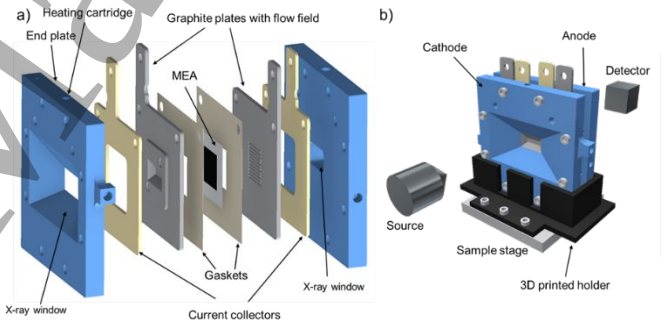

Figure 1 (a) Exploded view of the cell, including MEA, gaskets, graphite flow field plates and end-plates. The X-ray windows in the front and back end-plates allow for transmission of the beam in transmission mode while maintaining good compression in the region of study; b) the assembled cell sitting in the 3D printed holder on the beamline, with the direction of beam transmission from source to detector indicated (for transmission mode).

The cell setup positioned on the beamline is shown in Figure 2, with the front face of the cell shown in Figure 2 (a) and rear face of the cell in Figure 2 (b). Clearly shown on both cathode and anode are the imaging windows, with the wide bevel of the cathode imaging window shown in Figure 2 (a) for fluorescence mode acquisition. The X-ray window in the anode allows for acquisition in transmission mode, as was done throughout the experiments described here. The beam

path is also indicated, showing that the beam passes first through the cathode then through the anode before reaching the detector. Cathode and anode gas inlets were insulated to prevent water condensation, as shown in Figure 2 (b, left). Electrical connections to the current collectors on the top of the cell, as well as the heater connections and green thermocouple wire, are also seen in the images.

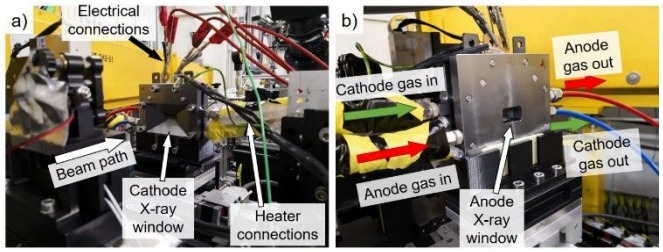

Figure 2 (a) Front-view and (b) rear-view of the cell on the beamline. The cathode and anode gas tubing is labelled in (b), showing the direction of gas flow through the cell. Electrical connections to current collectors on the top or the cell are indicated in (a), as well as the heater connection wires. Beam path is indicated in (a), with the cathode facing the source at the front and anode at the back.

Aqueous phase three-electrode measurements were conducted using a custom-designed electrochemical cell which has been previously presented by Wise et al. for use with *in situ* X-ray measurements (we will refer to this existing cell design as "*in situ*" in this work).[30] This cell has a platinum wire counter electrode out of the beam path and a port to allow reference electrode access for three-electrode electrochemical measurements (a Gaskatel HydroFlex® RHE was used in this work). 1 mol dm^{-3} $HClO_{4(aq)}$ was used as the electrolyte in the *in situ* cell and pumped through the cell during measurements to allow for removal of any formed bubbles in the solution, which can contribute to severe degradation of the XAS signal.

Cathode electrodes were prepared by spraying an ink (250 mg 20wt% Pt/C, 1.45 mL 11wt% Nafion, 75 mL deionised water and 75 mL IPA) onto carbon paper with a microporous layer (with hydrophobic treatment) (Freudenberg H23C7 GDL) until a loading of 1.15 mg_{Pt} cm^{-2} was reached. An automated robotic spray printer (Sonotek ExactaCoat) was used to achieve an even distribution of catalyst (vital for the spectroscopic measurements) and electrodes that performed well electrochemically given their high loading (and therefore susceptibility to mass transport limitations). For spectra collection, commercial electrodes (Johnson Matthey, UK) were used on the anode, with a loading of 0.1 mg_{Pt} cm^{-2} (combined with the cathode, referred to as the PtPt MEA in this work). An additional MEA comprising of a cathode with loading of 1.15 mg_{Pt} cm^{-2} and a palladium anode with a loading of 0.1 mg_{Pd} cm^{-2} was prepared, with the Pd deposited using the robotic spray printer (referred to here as the PtPd MEA). Electrodes were cut with dimensions of 2.2 cm × 2.2 cm and hot-pressed onto a Nafion-212 membrane (DuPont, USA) at a temperature of 130 °C and pressure of 400 psi for 3 min.

Polarisation curves were collected with increments of 0.02 A and 2 s per point, with a cut-off voltage of 0.3 V, and humidified gases on the anode (hydrogen) and cathode (air). The current density at 0.3 V is described here as the 'cut-off current density'. To collect CVs, the cathode gas was first switched from air to nitrogen and flowed until the cell voltage fell below 0.1 V. At this time, voltammograms were collected with a scan rate of 10 mV s^{-1}. Similar CV measurements were taken using the three-electrode *in situ* aqueous electrochemistry cell for comparison.

Time-resolved XAS data at the Pt L_3-edge were measured at the I20-EDE beamline in turbo-XAS mode for the *in-situ* cell and in EDE transmission for the *operando* cell. The loading of Pt in the *operando* cell gave an absorption jump of ~0.12 that was sufficient for measurements in transmission mode. In contrast, measurements with the in-situ cell were performed in fluorescence geometry, with the cell at 45 degrees to the beam. The intensity of the beam before (I_0) and after (I_t) the sample was measured using 15cm long ionization chambers (OKEN, Japan) filled with appropriate mixtures of argon/helium gas for 15% beam absorption at I_0 (0.14 bar of Ar and 1.66 bar of He) and 85% at I_t (1.68 bar of Ar and 0.12 bar of He). The beam emitted by the sample was measured in total fluorescence yield mode with a 500 μm thick and 35.2 mm diameter Passivated Implanted Planar Silicon (PIPS) Detector (Mirion Technologies).

3. Results and Discussion

The results of electrochemical testing are shown in Figure 3. Polarisation curves were measured using the cell both in the laboratory, coupled to a Scriber 850e test station (Figure 3 (a), blue triangles), and with the cell on the beamline (Figure 3 (a), purple diamonds and green diamonds for PtPt and PtPd MEAs, respectively). Comparing the PtPt MEAs, it was found that the performance of the cell during lab-based testing exceeded that of an MEA with identical electrode loadings tested on the beamline, with a higher cut-off current density of 589 mA cm^{-2} compared with 437 mA cm^{-2}, respectively. The reason for the lower performance is attributed to higher Ohmic losses, despite the higher OCV of the cell tested on the beamline. This is to be expected as the better humidification of the commercial test station will lead to improved membrane conductivity compared with the simple bubble humidification used at the beamline. However, the portable nature of the rig used for this work is a significant advantage over more permanent infrastructure systems since the rig can be easily erected/dismantled and transported between beamlines. Nevertheless, despite the modifications made to the cell design to allow for XAS spectral collection on the beamline (X-ray windows, modified flow fields and simplified

humidification), the *operando* cell performs well, with the expected polarisation performance and contributions from activation, Ohmic and mass transport losses inherent in fuel cell operation. This validates its use for obtaining *operando* spectroscopic data in a realistic working fuel cell environment, although it does highlight a general difficulty of performing *operando* experiments at beamlines as opposed to the lab environment. With dedicated hardware for electrochemical experiments installed at more beamlines across the world, these limitations may be mitigated in the future.

To avoid the Pt at the anode contributing to the overall XAS signal, previous studies have replaced the anode catalyst with Pd/C,[26] though full cell performance was not demonstrated in this example.[22] To investigate the effects of such substitution of the anode catalyst, polarisation curves of an MEA prepared with a platinum anode (PtPt, purple diamonds) and an MEA prepared with a palladium anode (PtPd, green triangles) are compared in Figure 3 (a). The performance of the PtPd MEA was found to be significantly worse than the PtPt MEA, with a cutoff current density of 136 mA cm^{-2} for the PtPd MEA compared with 437 mA cm^{-2} for the PtPt MEA. It is clear from the polarisation curve of the PtPd MEA that there were significant activation and Ohmic losses in the cell, contributing to the low performance and highlighting that, in terms of fuel cell performance, the use of Pd on the anode is not well suited.

Whereas the use of Pt on the anode is better suited for fuel cell performance, initial XAS experiments were carried out for both the PtPt and PtPd MEAs to ensure that the small amount of Pt on the anode did not interfere with the signal (as it would be in the path of the beam). It would be expected that the Pt on the anode would display the characteristics of Pt metal (Pt^0), which could then lead to an underestimation of the amount of oxidation when the cathode is at more positive potentials. A low loading Pt anode was used to minimise this effect (<10% of the cathode loading). Comparison between spectra collected with the Pt -anode (PtPt MEA) and the Pd -anode (PtPd MEA) showed a small difference in the Pt signal of the XAS, as shown in Figure 4 (a). However, the PtPd MEA actually showed less Pt cathode oxidation, which could be due to a worse electrochemical performance (Figure 4 (b)). The counter electrode in these two-electrode MEA CV experiments is the anode electrode, which in both cases is significantly lower loading (and therefore lower electrochemical surface area) than the working (cathode) electrode; this is not problematic for the very fast kinetics of the HOR/HER on the Pt anode, but for the Pd anode a significant overpotential exists, meaning that at the highest potential in the CV (1.2 V) the Pt cathode is actually less oxidised in the case of the PtPd MEA than the PtPt MEA, resuling in a lower white line intensity for the former. The PtPt MEA would be expected to show slightly lower total oxidation due to the contribution from the Pt^0 of the anode, and some evidence for this small effect is seen when comparing the XANES of the PtPt MEA with that of the Pt *in situ* cell (which has no anode/counter electrode in the beam path, Figure 5 (b)). The spectra for 50 mV unsurprisingly overlay each other. Together with the poor electrochemistry of the Pd anode, it was deemed that a low loading of 0.1 mg_{Pt} cm^{-2} on the anode provided the best option for both electrochemical performance and spectral acquisition.[31,32] It has been shown that small amounts of Pt alloyed with Pd can drastically improve the performance of the anode in PEM fuel cells, and such an anode catalyst would be an option for future experiments. However, only a slight influence of the anode Pt in the spectra was observed, due to the order of magnitude lower loading of the anode compared to the cathode. Hence, the presence of Pt on the anode is not thought to be critical for these measurements.[33]

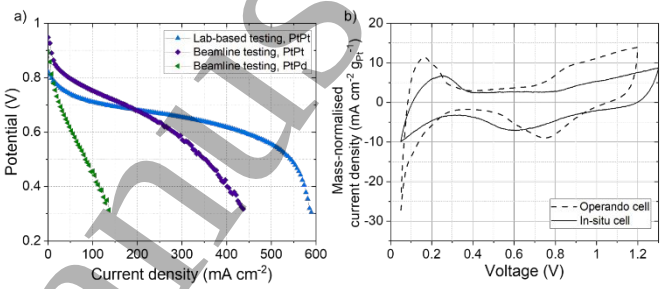

Figure 3 (a) Polarisation curves of MEAs tested at 50°C in the laboratory using the commercial test rig (blue) versus at 50 °C on the beamline during acquisition. The PtPt (purple) and PtPd (green) curves both had MEAs with loadings of 1.15 mg_{Pt} cm^{-2} on the cathode, with a platinum anode on the PtPt MEA (0.1 mg_{Pt} cm^{-2}, purple) and a palladium anode on the PtPd MEA (0.1 mg_{Pd} cm^{-2}, green); (b) Mass-normalised CV curve at 10 mV s^{-1} of the beamline-tested MEA (1.15 mg_{Pt} cm^{-2}) in the operando cell and catalyst coated carbon paper (0.45 mg_{Pt} cm^{-2}) in the in situ cell.

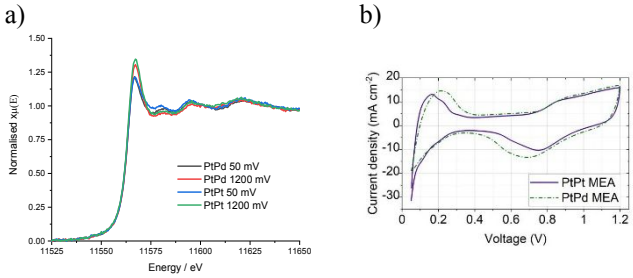

Figure 4 (a) Normalised XANES spectra for 0 V and 1.2 V for each anode electrode (Pt and Pd); (b) CV curves at 10 mV s^{-1} of the beamline-tested MEAs for each anode electrode (Pt and Pd).

Figure 3 (b) compares the performance of the *operando* fuel cell (dashed line) to that of the existing *in situ* cell (solid line). The *operando* cell was operating in CV mode, where the cathode has a flow of N_2 and the anode a flow of H_2 acting as

both a reference and counter electrode. Both datasets have been mass-normalised to account for the varying platinum loading of the electrodes. The CV performance of the *operando* cell (Figure 3 (b), dashed line), which it should be emphasised is employing a solid polymer electrolyte and humidified gases in a two-electrode set-up, compared to the *in situ* cell (Figure 3 (b), solid line), which uses an aqueous acid electrolyte and vacuum filled electrodes in a three-electrode setup, is highly encouraging. The characteristic features of the Pt catalyst electrode are all observed in the CV, including distinct hydrogen ads-/desorption peaks at low voltages and Pt oxide formation and stripping peaks at high voltages, further validating the design of the *operando* cell.

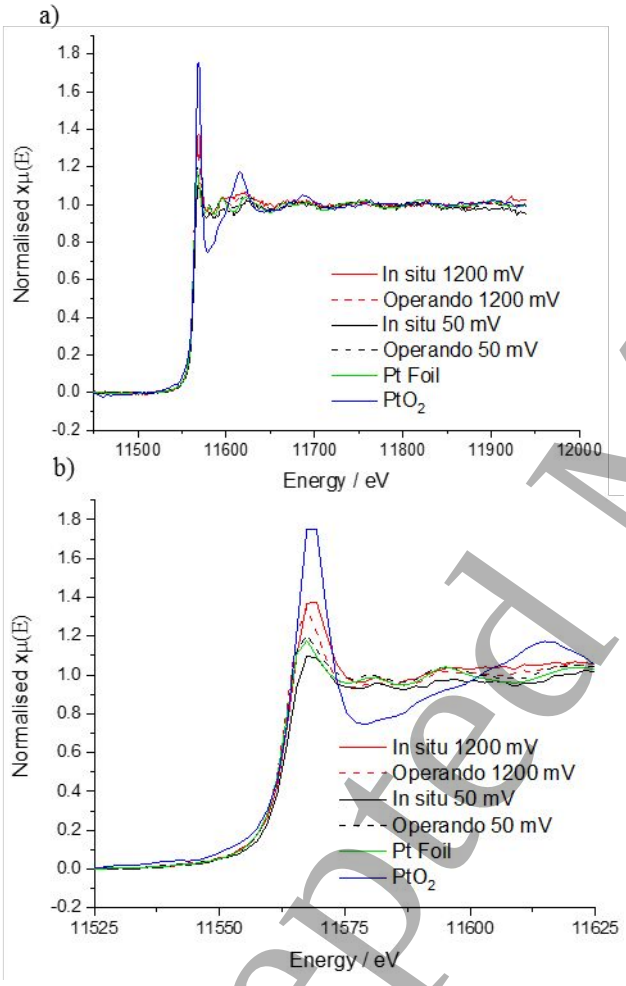

Figure 5. Normalised spectra for 0 V and 1.2 V in each cell compared to the two references used for the LCF presented in Figure 6; (a) showing the whole spectra and (b) highlighting the XANES region. In situ cell operated in turbo-XAS mode and the operando cell operated in transmission mode.

To benchmark the spectroscopic performance of the cell, spectra were collected during electrochemical cycling at 10 mV s^{-1} using each of the cells. The cells were scanned from 0.05 V to 1.2V vs RHE (the *in situ* cell was cycled up to 1.25 V *vs* RHE, shown in Figure 3). shows representative spectra collected from each cell (at 0.05 V *vs* RHE) as well as spectra from the two reference samples (Pt and PtO2) which were used to complete the linear combination fitting (LCF) displayed in Figure 6. In Figure 5, the cells are at the most reducing potential and therefore it is unsurprising that the spectra are most similar to the Pt foil reference. These results provide confidence that the two cells give similar results when measuring fuel cell catalysts and the data quality is comparable (spectra for each were collected over 5 seconds). Although data collection at shorter time scales has been previously demonstrated, these works have either used an "*in situ*" enviroment which doesn't benefit from the realistic conditions of fuel cell operation, or used an "*operando"* cell with kapton windows, which we believe will comprimise the area of measurement due to a lack of structrual compression and electrical conductivity, both issues are countered by using graphite plates as in the "*operando*" cell design presented here. Figure 6 shows the results of the linear combination fitting for the two whole datasets (using DAWN data processing software) and it is very encouraging that the results are similar.[34] There is, however, an offset between the two experiments, with the *operando* cell showing more Pt foil (Pt^0) characteristics throughout, which may be attributed to the increased thickness of the electrodes used for the *operando* electrochemical cell, or from the contributions of H_2 crossing over from the anode side of the MEA, further reducing the Pt catalyst. The increase in thickness results in a corresponding decrease in the mass transport through the catalyst layer, with some of the electrode signal lagging behind the voltage peak.[35] Some recent work has shown that this picture is complicated by different operating conditions (humidity, gas flow rates, current density, etc.) as well as the details of the catalyst layer design.[36] It has been shown that thick electrodes have a high electrolyte Ohmic resistance due to the ionomer network pathway in the electrode, even if in some cases moderate thickness electrodes can actually have lower mass transport resistance than thin electrodes due to the presence of water in the former.[37] The ionomer solution in the catalyst ink used to manufacture the electrode is the only pathway of electrolyte connectivity through the thickness of the electrode for the *operando* cell. For the *in situ* cell, the lower loading of the catalyst layer and use of an aqueous electrolyte creates the ionic pathways through the whole electrode, which lead to less sluggish electrochemical performance compared to the use of solid electrolyte ionic conductivity in the *operando* cell. Finally, there is also a contribution from the counter electrode, as described above, which is manifest as a possible Pt^0 signal (due to the low

potential and H_2 gas present on that electrode). The *in situ* cell uses a counter electrode which is not in the path of the beam and therefore it does not need to be considered when comparing the spectra.

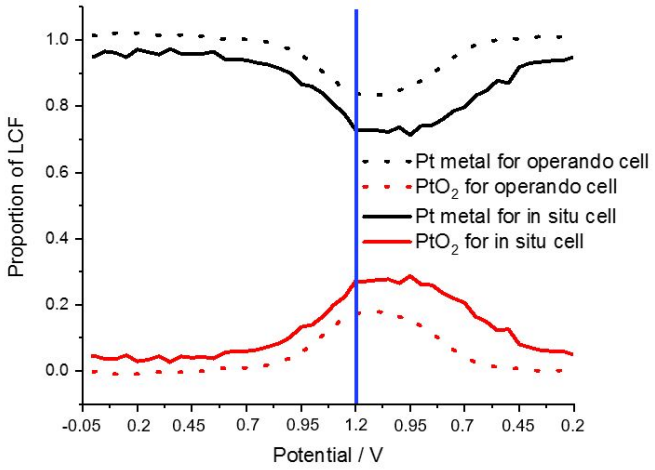

Figure 6: Linear combination fitting (LCF) results for the two cells during a cyclic voltammogram experiment with the cells cycled between 0.05-1.2 V (the in situ cell was cycled up to 1.3 V) vs RHE at 10 mV s-1(the blue line shows the point in time where the cells reached the upper voltage of 1.2 V vs RHE). Data between 1.2 and 1.3 V has been omitted for this comparison. A two-component fit (Pt foil and PtO_2 pellet) was used. The dotted lines show the results for the operando cell and the solid lines show the results for the in situ cell. The black lines show the proportion of the fit accounted for by Pt foil and the red lines the proportion of the fit accounted for by the PtO_2. Electrochemical data are presented in Figure 3 (b). Spectra collected every 5 seconds for both cells.

The results described thus far only consider the XANES region of the absorption spectrum. This provides information about the oxidation state of the catalyst, but geometrical structural information can be obtained by the analysis of the EXAFS region. The background-subtracted k^2 weighted EXAFS signals are shown in Figure 7, and illustrate that the EXAFS oscillations extend to $k > 8$, that is indicative of Pt-Pt coordination. The signal quality limits the analysis range to k = 12 Å^{-1}, while previous work has shown that 14 Å^{-1} is preferred for drawing firm conclusions from the EXAFS in Pt catalysts.10

These spectra obtained every 5 s, with electrochemical cycling at 10 mV s^{-1} demonstrate that the cell is suitable for *operando* spectroscopy, and thus it could find wider application on QuickEXAFS beamlines, and in particular on the latest generation of very fast QEXAFS beamlines that could allow for the acquisition speeds necessary to study transient behaviour whilst also providing EXAFS data of sufficient quality to extract detailed structural information. Additionally, the results presented here are a significant improvement on previous published *operando* measurements, using a dispersive X-ray beam, where a range of up to k=8 Å^{-1} was achieved.[38]

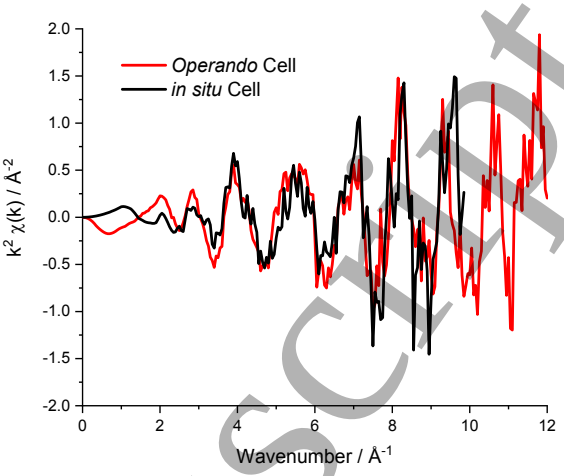

Figure 7. k-space EXAFS data (k^2 weighted) for the two different cells, calculated from the same data presented in Figure 5.

4.Conclusions and Future Work

This work has presented a new *operando* cell design which maximises both the electrochemical performance and the XAS data quality in an operating fuel cell environment. The cell's performance as a fuel cell in the idealised laboratory environment and on the beamline has been demonstrated, illustrating the effects of the reduced humidification available at the beamline on the cell performance. This novel cell has been compared to an established three-electrode aqueous cell, and it has been shown to provide similar quality XAS data and cyclic voltammetry performance. It has also been shown be able to operate as a fuel cell under beam irradiation, providing an avenue for fully *operando* measurements during fuel cell operation in the future. These measurements would benefit from standardised humidification and heating of the fuel cell being available at the beamline, but are possible with the current apparatus. Turbo-XAS acquisition every 5 s was shown to produce the same trend in the Pt^0 and PtO_x contributions during the cyclic voltammogram for both cell environments, demonstrating both the beamline and the cell's capability for rapid acquisition of XAS and electrochemical data. Future work will seek to use this fuel cell design to study transient effects in real operating conditions of the fuel cell with gas-phase reactions and solid electrolyte membranes,

elucidating the changes that the catalysts undergo during reaction in operating fuel cells.

Acknowledgements

The authors acknowledge Diamond Light Source for the time on beamline I20-EDE under proposals SP22008 and SP15650. PFM, DJLB, PS and MCW have received funding from the EU Graphene Flagship under Horizon 2020 Research and Innovation program grant agreement no. 881603-GrapheneCore3 and from the EPSRC Materials Research Hub for Energy Conversion, Capture, and Storage (M-RHEX) EP/R023581/1. Paul Shearing acknowledges the Royal Academy of Engineering (CiET1718/59) for financial support. The authors would like to acknowledge funding from the EPSRC (EP/L015277/1, EP/P009050/1, EP/M014371/1, EP/M009394/1, EP/M023508/1, EP/L015749/1, EP/N022971/1, EP/S01800X/1) for supporting fuel cell research in the Electrochemical Innovation Lab (EIL). TSM would also like to thank the EPSRC for support via his Fellowship EP/P023851/1. AER acknowledges support of the Johnson Matthey Technology Centre during the development of the *in situ* cell. JH acknowledges a studentship from the EPSRC Centre for Doctoral Training in Advanced Characterisation of Material (EP/LO15277/1).

References

[1] Borup R L, Kusoglu A, Neyerlin K C, Mukundan R, Ahluwalia R K, Cullen D A, More K L, Weber A Z and Myers D J 2020 *Curr. Opin. Electrochem.* **21** 192–200

[2] Anon DOE Hydrogen Program: 2019 Annual Progress Report - Fuel Cell R&D

[3] Russell A E and Rose A 2004 *Chem. Rev.* **104** 4613–35

[4] Ball S C, Hudson S L, Leung J H, Russell A E, Thompsett D and Theobald B R 2019 *ECS Trans.* **11** 1247–57

[5] Kaito T, Tanaka H, Mitsumoto H, Sugawara S, Shinohara K, Ariga H, Uehara H, Takakusagi S and Asakura K 2016 *J. Phys. Chem. C* **120** 11519–27

[6] Huang H, Nassr A B A A, Celorrio V, Taylor S F R, Puthiyapura V K, Hardacre C, Brett D J L and Russell A E 2018 *Faraday Discuss.* **208** 555–73

[7] Jackson C, Smith G T, Inwood D W, Leach A S, Whalley P S, Callisti M, Polcar T, Russell A E, Levecque P and Kramer D 2017 *Nat. Commun.* **8** 1–11

[8] Jackson C, Smith G T, Markiewicz M, Inwood D W, Leach A S, Whalley P S, Kucernak A R, Russell A E, Kramer D and Levecque P B J 2018 *J. Electroanal. Chem.* **819** 163–70

[9] Dent A J, Cibin G, Ramos S, Parry S A, Gianolio D, Smith A D, Scott S M, Varandas L, Patel S, Pearson M R, Hudson L, Krumpa N A, Marsch A S and Robbins P E 2013 *Journal of Physics: Conference Series* vol 430 (Institute of Physics Publishing) p 12023

[10] Mathew R J and Russell A E 2000 *Top. Catal.* **10** 231–9

[11] Sekizawa O, Uruga T, Higashi K, Kaneko T, Yoshida Y, Sakata T and Iwasawa Y 2017 *ACS Sustain. Chem. Eng.* **5** 3631–6

[12] Povia M, Herranz J, Binninger T, Nachtegaal M, Diaz A, Kohlbrecher J, Abbott D F, Kim B J and Schmidt T J 2018 *ACS Catal.* **8** 7000–15

[13] Diaz-Moreno S, Amboage M, Basham M, Boada R, Bricknell N E, Cibin G, Cobb T M, Filik J, Freeman A, Geraki K, Gianolio D, Hayama S, Ignatyev K, Keenan L, Mikulska I, Mosselmans J F W, Mudd J J and Parry S A 2018 *J. Synchrotron Radiat.* **25** 998–1009

[14] Diaz-Moreno S, Hayama S, Amboage M, Freeman A, Sutter J and Duller G 2009 *Journal of Physics: Conference Series* vol 190 (Institute of Physics Publishing) p 012038

[15] Dann E K, Gibson E K, Catlow C R A, Celorrio V, Collier P, Eralp T, Amboage M, Hardacre C, Stere C, Kroner A, Raj A, Rogers S, Goguet A and Wells P P 2019 *J. Catal.* **373** 201–8

[16] Pascarelli S, Neisius T and De Panfilis S 1999 *J. Synchrotron Radiat.* **6** 1044–50

[17] Alinejad S, Inaba M, Schröder J, Du J, Quinson J, Zana A and Arenz M 2020 *J. Phys. Energy* **2** 024003

[18] Zana A, Speder J, Roefzaad M, Altmann L, Bäumer M and Arenz M 2013 *J. Electrochem. Soc.* **160** F608–15

[19] Ferreira P J, la O' G J, Shao-Horn Y, Morgan D, Makharia R, Kocha S and Gasteiger H A 2005 *J. Electrochem. Soc.* **152** A2256

[20] Jervis R, Mansor N, Sobrido A J, Jones S, Gibbs C, Neville T P, Millichamp J, Shearing P R and Brett D J L 2017 *J. Electrochem. Soc.* **164** F1551–5

[21] Mayrhofer K J J, Strmcnik D, Blizanac B B, Stamenkovic V, Arenz M and Markovic N M 2008 *Electrochim. Acta* **53** 3181–8

[22] Matsui H, Ishiguro N, Uruga T, Sekizawa O, Higashi K, Maejima N and Tada M 2017 *Angew. Chemie Int. Ed.* **56** 9371–5

[23] Ishiguro N, Saida T, Uruga T, Nagamatsu S I, Sekizawa O, Nitta K, Yamamoto T, Ohkoshi S I, Iwasawa Y, Yokoyama T and Tada M 2012 *ACS Catal.* **2** 1319–30

[24] Ichihashi K, Muratsugu S, Matsui H, Higashi K, Sekizawa O, Uruga T and Tada M 2020 *J. Phys. Chem. C*

[25] Wiltshire R J K, King C R, Rose A, Wells P P, Hogarth M P, Thompsett D and Russell A E 2005 *Electrochimica Acta* vol 50 (Pergamon) pp 5208–17

[26] Burton S L 2009 *A comparative study of PtCo/C Alloys and Pt/C as cathode catalysts for fuel cell applications* (University of Southampton)

[27] Reksten A H, Russell A E, Richardson P W, Thompson S J, Mathisen K, Seland F and Sunde S 2020 *Phys. Chem. Chem. Phys.* **22** 18868–81

[28] Millichamp J, Mason T J, Neville T P, Rajalakshmi N, Jervis R, Shearing P R and Brett D J L 2015 *J. Power Sources* **284** 305–20

[29] Lochner T, Hallitzky L, Perchthaler M, Obermaier M, Sabawa J, Enz S and Bandarenka A S 2020 *Appl. Energy* **260** 114291

[30] Wise A M, Richardson P W, Price S W T, Chouchelamane G, Calvillo L, Hendra P J, Toney M F and Russell A E 2018 *Electrochim. Acta* **262** 27–38

[31] Papageorgopoulos D C, Keijzer M, Veldhuis J B J and de Bruijn F A 2002 *J. Electrochem. Soc.* **149** A1400

[32] Garcia A C, Paganin V A and Ticianelli E A 2008 *Electrochim. Acta* **53** 4309–15

[33] Antolini E, Zignani S C, Santos S F and Gonzalez E R 2011 *Electrochim. Acta* **56** 2299–305

[34] Basham M, Filik J, Wharmby M T, Chang P C Y, El Kassaby B, Gerring M, Aishima J, Levik K, Pulford B C

A, Sikharulidze I, Sneddon D, Webber M, Dhesi S S, Maccherozzi F, Svensson O, Brockhauser S, Náray G and Ashton A W 2015 *J. Synchrotron Radiat.* **22** 853–8

[35] Talukdar K, Delgado S, Lagarteira T, Gazdzicki P and Friedrich K A 2019 *J. Power Sources* **427** 309–17

[36] Schuler T, Chowdhury A, Freiberg A T, Sneed B, Spingler F B, Tucker M C, More K L, Radke C J and Weber A Z 2019 *J. Electrochem. Soc.* **166** F3020–31

[37] Antonacci P, Chevalier S, Lee J, Ge N, Hinebaugh J, Yip R, Tabuchi Y, Kotaka T and Bazylak A 2016 *Electrochim. Acta* **188** 888–97

[38] Achilli E, Minguzzi A, Lugaresi O, Locatelli C, Rondinini S, Spinolo G and Ghigna P 2014 *J. Spectrosc.* **2014** 480102